International Communications in Heat and Mass Transfer 120 (2021) 105027

Contents lists available at ScienceDirect

International Communications in Heat and Mass Transfer

journal homepage: www.elsevier.com/locate/ichmt

Non-magnetized mixed convective viscous flow submerged in titanium oxide and aluminum titanium oxide hybrid nanoparticles towards a surface of cylinder

Fazal Haq [a], M. Ijaz Khan [b], Yu-Ming Chu [c,d,*], Niaz B. Khan [e], Seifedine Kadry [f]

[a] Department of Mathematics, Karakoram International University Main Campus, Gilgit 15100, Pakistan
[b] Department of Mathematics, Riphah International University, Faisalabad Campus, Faisalabad 38000, Pakistan
[c] Department of Mathematics, Huzhou University, Huzhou 313000, PR China
[d] Hunan Provincial Key Laboratory of Mathematical Modeling and Analysis in Engineering, Changsha University of Science & Technology, Changsha 410114, PR China
[e] School of Mechanical and Manufacturing Engineering, National University of Sciences and Technology, Islamabad, Pakistan
[f] Department of Mathematics and Computer Science, Beirut Arab University, Beirut, Lebanon

ARTICLE INFO

Keywords:
Hybrid nanofluid
Stretching cylinder
Porous medium
Thermal radiation
Heat generation
Stagnation point

ABSTRACT

Hybrid nanofluids are novel fluids created by suspending two or more dissimilar nano sized particles in base fluids. Thermal conductivity of hybrid nanofluids is more than nanofluids. Now a day, due to high thermal conductivity and applications in engineering and industry, hybrid nanofluids have become attractive area of research for scientist and researchers. The main objective of current communication is to study the stagnation point flow and heat transfer in viscous hybrid nanofluid towards a stretched cylinder. Flow characteristics are examined under the effect of magnetic field and mixed convention. Furthermore, energy communication is constructed considering thermal radiation, uniform heat source and viscous dissipation. The obtained governing dimensional model is transformed into ordinary ones using suitable transformations. ND-solve code is used to tackle the ordinary differential equations. Results are discussed and compared subject to nanofluid and hybrid nanofluid and plotted graphically. Moreover, Nusselt number and skin friction coefficient are studied numerically. Key outcomes are highlighted at the end.

1. Introduction

Hybrid nanofluids are novel fluids, engineered by colloidal suspension of two or more dissimilar nano sized particles of oxides or metals into base fluid like water and ethylene glycol, propylene glycol, triethylene and kerosene oil. Hybrid nanofluid is an advanced type of nanofluid which is used for enhancement of thermal conductivity of conventional nanofluids. Due to high thermal conductivity and vital applications in engineering and industry such as solar heating, micro fluidics, heat transportation, medical manufacturing, lubrication, generator cooling, acoustics defense and naval structures hybrid nanofluids attracted the attention of numerous scientists and researchers. Devi and Devi [1] presented a mathematical model for MHD hybrid nanofluid ($Cu - Al_2O_3/H_2O$) with suction. The effects of transpiration on hybrid nanofluid ($Cu - Al_2O_3/H_2O$) and heat transport over extending/shrinking surface taking uniform shear flow is reported by Waini et al. [2]. Khan et al. [3] studied the flow behavior of MHD hybrid nanofluid ($SiO_2 - MoS_2/C_3H_8O_2$) subject to viscous dissipation and heat generation with entropy optimization. Boundary layer flow of dusty hybrid nanofluid ($Cu - Al_2O_3/H_2O$) flow over stretching permeable surface with variable thermal conductivity and thermal radiation is reported by Ghadikolaei et al. [4]. Maskeen et al. [5] explored the heat transfer enhancement in MHD alumina--copper hybrid nanofluid flow over stretched surface of cylinder taking pure water as base fluid. Some recent advancement in this connection is enlisted in references [6–12].

Stagnation point flow in fluid is the instant region of hard surface at which fluid approaching the surface splits into diverse streams. Such type of flows has broadly been applied in technological and industrial zones since it has maximum fluid pressure, heat transfer and mass deposition rate in neighborhood of stagnation point. Analysis of stagnation point flow and stability in hybrid nanofluid under the influence of source effects over extending/shrinking sheet is reported by Kamal et al. [13]. Fadhilah et al. [14] explore the heat transfer and stagnation point flow in unsteady nanofluid over exponentially stretching/shrinking sheet having porous surface with slip velocity impact. Stagnation point

* Corresponding author at: Department of Mathematics, Huzhou University, Huzhou 313000, PR China.
E-mail address: chuyuming@zjhu.edu.cn (Y.-M. Chu).

https://doi.org/10.1016/j.icheatmasstransfer.2020.105027

Available online 21 November 2020

Nomenclature

u, v	Velocity components
u_0, b	Stretching constants
ρ_{hnf}	Density
μ_{hnf}	Dynamic viscosity
β_{hnf}	Coefficient of thermal expansion
g	Gravity acceleration
K_p	Permeability
$(\rho C_p)_{bf}$	Heat capacity of base nanofluid
$(\rho C_p)_{hnf}$	Heat capacity of hybrid nanofluid
Q_0	Heat generation coefficient
K_1	Permeability parameter
U_e	Free stream velocity
Nt	Thermophoresis parameter
h_w	Heat flux
k_{hnf}	Thermal conductivity
Gr	Grashof number
Rd	Radiation parameter
Ec	Eckert number
C_{fx}	Coefficient of skin friction
Al_2O_3	Aluminum Oxide
τ_w	Shear stress
ϕ_1, ϕ_2	Volume fraction of nano and hybrid nanoparticles
r, x	Cylindrical coordinates
R	Radius of cylinder
K^*	Curvature parameter
l	Characteristic length
σ^*	Boltzmann constant
T_∞	Ambient temperature
η	Dimensionless variable
T_W	Wall temperature
Re	Reynolds number
β^*	Heat generation parameter
U_w	Stretching velocity
Pr	Prandtl number
J_w	Mass flux
Nb	Brownian motion parameter
Gt	Mixed convection parameter
τ	Capacity ratio
f, θ	Dimensionless velocity, temperature
Nu_x	Nusselt number
K^{**}	Mean absorption coefficient
TiO_2	Titanium Oxide
B	Velocity ratio parameter
hnf	Stands for hybrid nanofluids

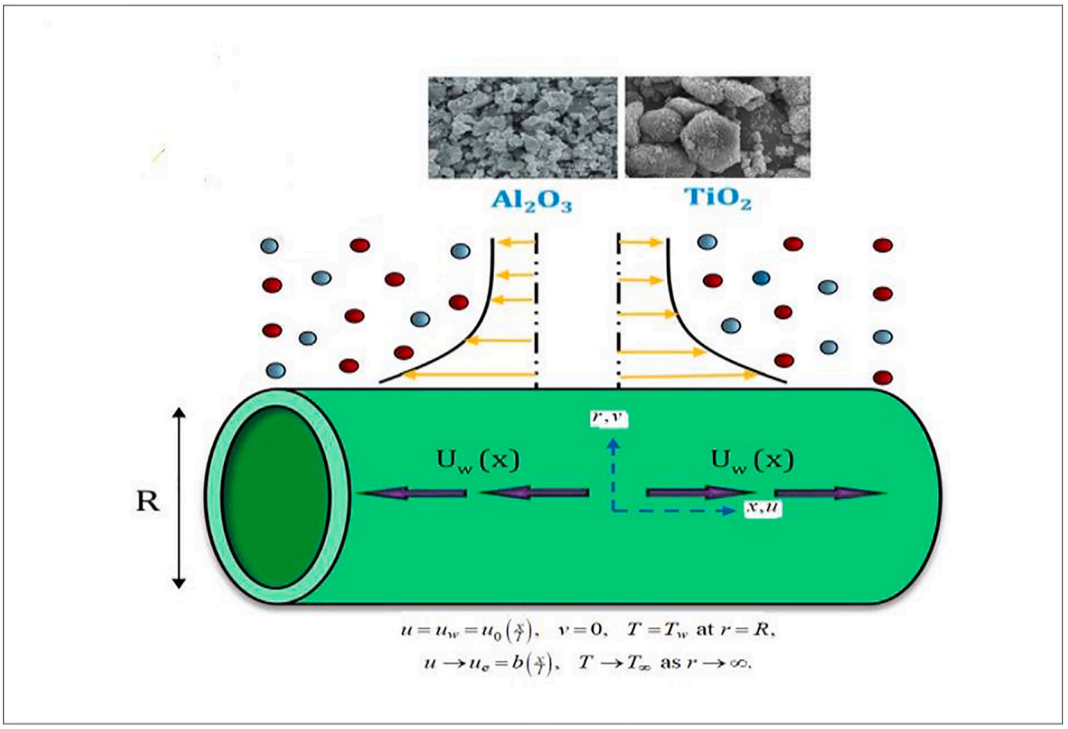

Fig. 1. Schematic flow diagram.

flow with mixed convective and Darcy-Fochheimer effects over porous surface of cylinder is investigated by Hayat et al. [15]. Yousefi et al. [16] studied stagnation point flow in hybrid nanofluid (titania-copper) over a wavy cylinder. Behavior of $(Cu - Al_2O_3/H_2O)$ hybrid nanomaterial flow near stagnation point over stretching/shrinking cylinder is examined by Waini et al. [17]. Ahmed et al. [18] reported heat transfer in three dimensional radiative stagnation point flow of hybrid nanofluid.

Fluid flows through porous surface have received attention of researchers and scientists in last several decades. It has numerous applications in engineering such as passage of contaminants in soil and underground water, oil recovery, composites processing, chromatography, filtration and chemical reaction engineering. Keceioglu and Jiang [19] studied flow of packed spheres coated by water over porous surface. Characteristics of copper oxides nanoparticles suspended in pure water flow over porous wavy surface is investigated by Hassan et al. [20]. Mehryan et al. [21] reported heat transfer enhancement in hybrid nanofluid flow over porous surface with magnetic field and convection effects. Flow behavior of $(Ag - MgO/H_2O)$ hybrid nanofluid over a

Table 1
Physical properties of pure water (H_2O), Titanium oxide (T_iO_2) and Aluminum oxide (Al_2O_3) [5, ⇄9].

	$K(w/mK)$	$\rho(Kgm^3)$	$C_p(J/KgK)$	$\beta \times 10^{-6}(K^{-1})$
Pure water (H_2O)	0.613	997.1	4179	210
Titanium oxide (T_iO_2)	8.9538	4250	686.2	9.0
Aluminum oxide (Al_2O_3)	40	3970	765	8.5

Table 2
Thermophysical properties of single and hybrid nanofluid [25,26].

Nanofluid ($T_iO_2 - H_2O$)	
Viscosity	$\mu_{nf} = \frac{\mu_{bf}}{(1-\phi_1)^{2.5}}$
Density	$\rho_{nf} = \rho_{bf}(1-\phi_1) + \rho s_1 \phi_1$
Thermal expansion coefficient	$(\rho\beta)_{nf} = (\rho\beta)_{bf}(1-\phi_1) + (\rho\beta)_{s_1}\phi_1$
Heat capacity	$(\rho C_p)_{nf} = (\rho C_p)_{bf}(1-\phi_1) + (\rho C_p)_{s_1}\phi_1$
Thermal conductivity	$\frac{K_{nf}}{K_f} = \frac{Ks_1 + K_{bf}(m-1) - (m-1)⇄(K_{bf} - Ks_1)⇄\phi_1}{Ks_1 + K_{bf}(m-1) + (K_{bf} - Ks_1)⇄\phi_1}$
Hybrid Nanofluid ($T_iO_2 - Al_2O_3/H_2O$)	
Viscosity	$\mu_{hnf} = \frac{\mu_{bf}}{(1-\phi_1)^{2.5}(1-\phi_2)^{2.5}}$
Density	$\rho_{hnf} = (1-\phi_2)⇄\{\rho_{bf}(1-\phi_1) + (\rho s_1)\phi_1\} + \rho s_2\phi_2$
Thermal expansion coefficient	$(\rho\beta)_{hnf} = (1-\phi_2)\left((\rho\beta)_{bf}(1-\phi_1) + (\rho\beta)_{s_1}\phi_1\right) + (\rho\beta)_{s_2}\phi_2$
Heat capacity	$(\rho C_p)_{hnf} = (1-\phi_2)\left((\rho C_p)_{bf}(1-\phi_1)⇄+ (\rho C_p)_{s_1}\phi_1\right) + (\rho C_p)_{s_2}\phi_2$
Thermal conductivity	$\frac{K_{hnf}}{K_{bf}} = \frac{Ks_2 + K_{bf}(m-1) - (m-1)(K_{bf} - Ks_2)\phi_2}{Ks_2 + K_{bf}(m-1) + (K_{bf} - Ks_2)\phi_2}$, where $\frac{K_{bf}}{K_f} = \frac{Ks_1 + K_f(m-1) - (m-1)⇄(K_f - Ks_1)\phi_2}{Ks_1 + K_f(m-1) + (K_f - Ks_1)\phi_2}$

horizontal channel with porous walls is studied by Jarray et al. [22]. Aladdin et al. [23] explored the features of $(Cu - Al_2O_3/H_2O)$ hybrid nanofluid flow over the moving porous surface taking MHD and suction effects.

Here comparative study of single and hybrid nanofluid with viscous dissipation, thermal radiation, heat generation and stagnation point flow over porous surface of stretched cylinder is investigated. Boundary layer assumptions are used to obtain the dimensional flow model. Suitable transformations are used to convert the dimensional model to non-dimensional one. NDsolve code in Mathematica software is used to tackle the flow expressions.

2. Problem formulation

The aim of current study is to investigate the stagnation point flow in two dimensional boundary layer $(TiO_2 - Al_2O_3/H_2O)$ hybrid nanofluid over stretching cylinder with porous surface. The axial and radial co-ordinates of cylinder are represented by $(x, ⇄r)$. The schematic flow diagram is displayed in Fig. 1. The impacts of mixed convection, thermal radiation, viscous dissipation and heat generation are taken into account. The governing flow expressions are [&,5,8,24]:

$$\frac{\partial}{\partial x}(ru) + \frac{\partial}{\partial r}(rv) = 0, ⇄ \tag{1}$$

$$\rho_{hnf}\left(u\frac{\partial u}{\partial x} + v\frac{\partial u}{\partial r}\right) = \mu_{hnf}\left[\frac{\partial^2 u}{\partial r^2} + \frac{1}{r}\frac{\partial u}{\partial r}\right] + U_e\frac{\partial U_e}{\partial x} - \frac{\mu_{hnf}}{K_p}(u - U_e) + g(\rho\beta)_{hnf}(T - T_\infty), ⇄ \tag{2}$$

$$\left.\begin{aligned}\frac{(\rho C_p)_{hnf}}{(\rho C_p)_{bf}}\left(u\frac{\partial T}{\partial x} + v\frac{\partial T}{\partial r}\right) = \frac{K_{hnf}}{(\rho C_p)_{bf}}\left[\frac{\partial^2 T}{\partial r^2} + \frac{1}{r}\frac{\partial T}{\partial r}\right] + \frac{16\sigma^* T_\infty^3}{3K^{**}}\frac{1}{(\rho C_p)_{bf}}\frac{\partial^2 T}{\partial r^2}\\ + \frac{\mu_{hnf}}{(\rho C_p)_{bf}}\left(\frac{\partial u}{\partial r}\right)^2 + \frac{Q_0}{(\rho C_p)_{bf}}(T - T_\infty),\end{aligned}\right\} \tag{3}$$

with

$$\left.\begin{aligned}u = U_w = u_0\left(\frac{x}{l}\right), ⇄v = 0, ⇄T = T_w \text{ at } r = R,\\ u \to U_e = b\left(\frac{x}{l}\right), ⇄T \to T_\infty \text{ as } r \to \infty.\end{aligned}\right\}⇄ \tag{4}$$

Table 1 and 2 are drawn for thermophysical properties of hybrid nanofluid.

In order to convert the system of PDE's (1 − 3), into ODE's we take the following transformations

$$\left.\begin{aligned}\eta = \frac{r^2 - R^2}{2R}\sqrt{\frac{u_0}{l\nu_f}}, ⇄u = u_0\left(\frac{x}{l}\right)⇄f'(\eta),\\ v = -\frac{R}{r}\sqrt{\frac{u_0\nu_f}{l}}f(\eta), ⇄\theta(\eta) = \frac{T - T_\infty}{T_w - T_\infty}.\end{aligned}\right\}⇄ \tag{5}$$

Using Eq. (5), Eq. (1) satisfied identically while Eqns. (2 − 4) take the form

$$A_1\{(1 + 2K^*\eta)⇄f''' + 2K^*f'' - (K_1 - B)f'\} + A_2\{ff'' - (f')^2\} + A_3G_t\theta + B^2 = 0, \}⇄ \tag{6}$$

$$A_4(1+2K^*\eta)⇄(\theta'' + 2K^*\theta') + Rd(\theta'' + K^*\theta') + PrA_1Ec(1+2K^*\eta)⇄f''^2 + Pr\beta^*\theta + A_5Prf\theta' = 0, \Big\}⇄ \tag{7}$$

with

$$\left.\begin{aligned}f(\eta) = 0, ⇄f'(\eta) = 1, ⇄\theta(\eta) = 1 \text{ at } \eta = 0,\\ f'(\eta) \to B, ⇄\theta(\eta) \to 0, ⇄\text{as } \eta \to \infty.\end{aligned}\right\}⇄ \tag{8}$$

The dimensionless parameters appearing in Eqs. (10 − 12) are mathematically defined as;

$$\left.\begin{aligned}K^* = \frac{1}{R}\sqrt{\frac{vl}{u_0}}, ⇄K_1 = \frac{vl}{k^* u_0}, ⇄Pr = \frac{\mu_f(C_p)_f}{K_f}, ⇄Re = \frac{u_0 x}{\nu}, ⇄Gr = \frac{g\beta(T_w - T_\infty)⇄x^3}{\nu^2},\\ Gt = \frac{Gr}{Re^2}, ⇄Ec = \frac{U_w^2}{(C_p)_f(T_w - T_\infty)}, ⇄Rd = \frac{16\sigma^* T_\infty^3}{3K^{**}K_f}, ⇄\beta^* = \frac{Q_0 l}{u_0(\rho C_p)_f},\\ B = \frac{b}{u_0}.\end{aligned}\right\} \tag{9}$$

2.1. Coefficient of skin friction and Nusselt number

The mathematical form of essential engineering quantities of practical interest i.e. Nusselt number (Nu_x) and skin friction coefficient (Cf_x) are expressed as follows:

where

$$\left.\begin{aligned}\tau_w = \mu_{hnf}\left(\frac{\partial u}{\partial r}\right)_{r=R}, ⇄\\ q_w = -k_{hnf}\left(\frac{\partial T}{\partial r}\right)_{r=R} - \frac{16\sigma^* T_\infty^3}{3K^{**}}\left(\frac{\partial T}{\partial r}\right)_{r=R}, ⇄\end{aligned}\right\}⇄ \tag{10}$$

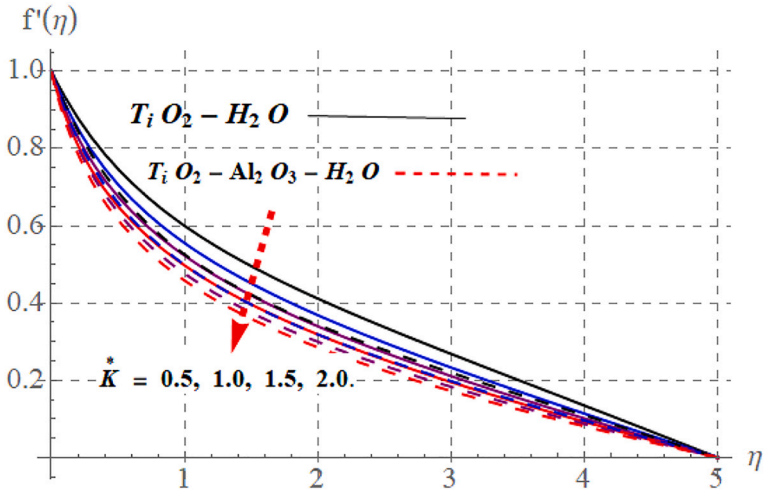

Fig. 2. $f'(\eta)$ versus K^*.

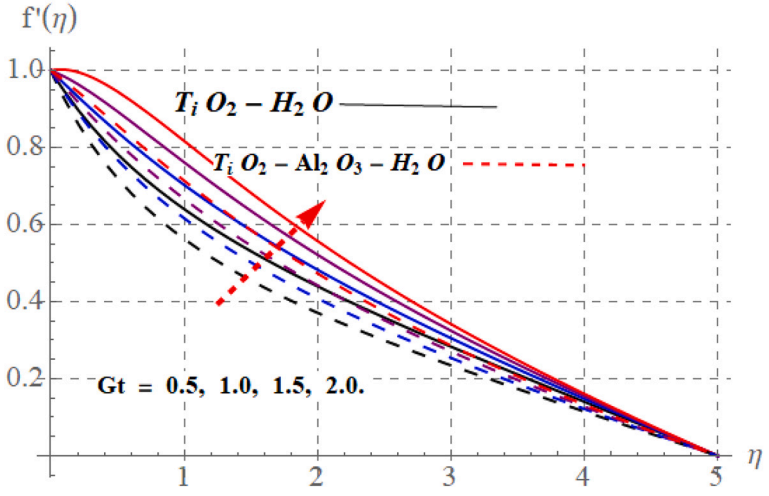

Fig. 3. $f'(\eta)$ versus Gt.

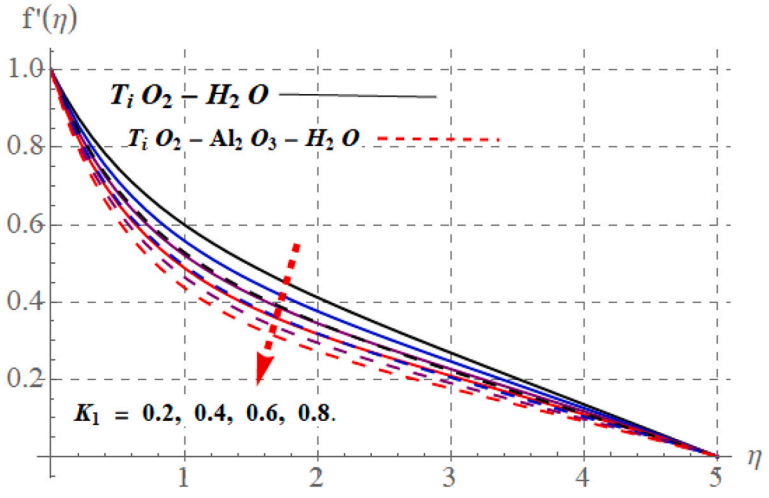

Fig. 4. $f'(\eta)$ versus K_1.

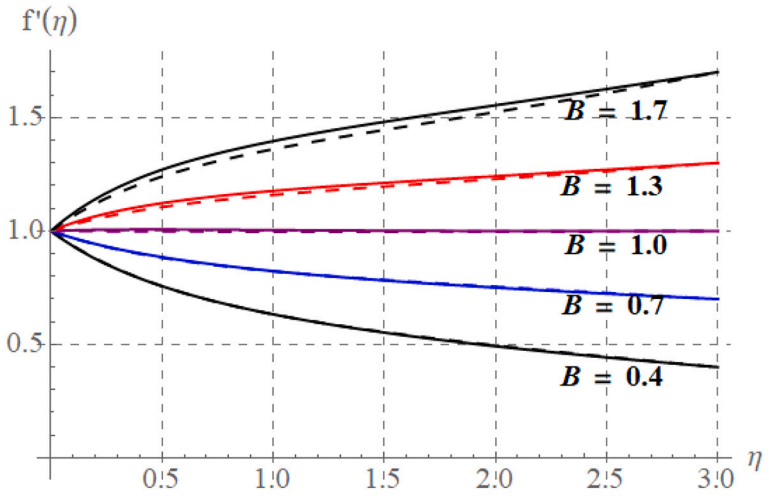

Fig. 5. $f'(\eta)$ versus B.

finally

$$\left.\begin{aligned}(Re)_x^{0.5} Cf_x &= A_1 f''(0),\\ \mathrm{Re}_x^{-0.5} Nu_x &= -(A_4 + R)\theta'(0),\end{aligned}\right\} \rightleftarrows \tag{11}$$

where $\mathrm{Re}_x \left(= \sqrt{\frac{x^2 u_0}{\nu l}} \right)$ is local Reynolds's number.

Constant terms appearing in above equations are defined as;

$$\left.\begin{aligned}A_1 = \frac{\mu_{hnf}}{\mu_{bf}}, \rightleftarrows A_2 = \frac{\rho_{hnf}}{\rho_{bf}}, \rightleftarrows A_3 = \frac{(\rho\beta)_{hnf}}{(\rho\beta)_{bf}},\\ A_4 = \frac{K_{hnf}}{K_f}, \rightleftarrows A_5 = \frac{(\rho C_p)_{hnf}}{(\rho C_p)_{bnf}}.\end{aligned}\right\} \tag{12}$$

3. Results and discussion

Here Newton built in shooting method is used to obtain the graphical and numerical results of system ODE's (6) & (7) with boundary conditions (8). Salient behavior of pertinent flow controlling parameters on momentum and temperature is discussed for both single and hybrid nanofluids. Nusselt number and skin friction coefficients are computed numerically for nanofluid and hybrid nanofluid. Computations are carried out by taking $K^* = \mathrm{Pr} = Rd = 0.5, K_1 = Ec = \beta^* = Gt = 0.2, B = 0.4$, $\phi_1 = \phi 2 = 0.05, m = 5.3$.

3.1. Velocity

In this sub section, physical impact of flow controlling variables like curvature (K^*), convection (G_t), porosity (K_1) and stagnation point (B) on velocity field ($f'(\eta)$) is studied through Figs. ($2-5$). The impact of curvature parameter on single and hybrid nanofluid is depicted in Fig. 2. One can observe from this figure that $f'(\eta)$ diminishes via rising K^*. It is due to the fact that when curvature increases, radius of cylinder reduces, consequently contact area between surface of cylinder and fluid decays. Thus fluid velocity near cylinder reduces. Fig. 3 is sketched to study the effect of convection parameter on velocity. Clearly, higher Gt causes upsurge in velocity field. Physically, the temperature difference between surface and ambient fluid enhances via rising Gt, due to which temperature gradient is generated. Hence velocity field increases for higher G_t. Fig. 4 is delineated to observe the infiltration in velocity via porosity variable. Reduction in velocity is observed from Fig. 4. Since permeability produces resistive force which opposes the flow. Thus velocity decays for both single and hybrid nanofluids. The flow behavior of stagnation point in single and hybrid nanofluids is depicted in Fig. 5. From this figure one can notice that the boundary layer vanishes for $B = 1$, while for $B > 1$, velocity enhances and in case of $B < 1$, velocity decreases.

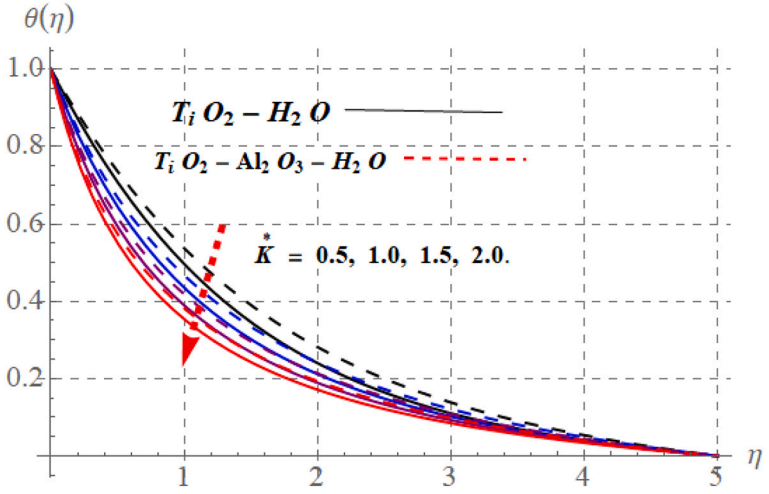

Fig. 6. $\theta(\eta)$ versus K^*.

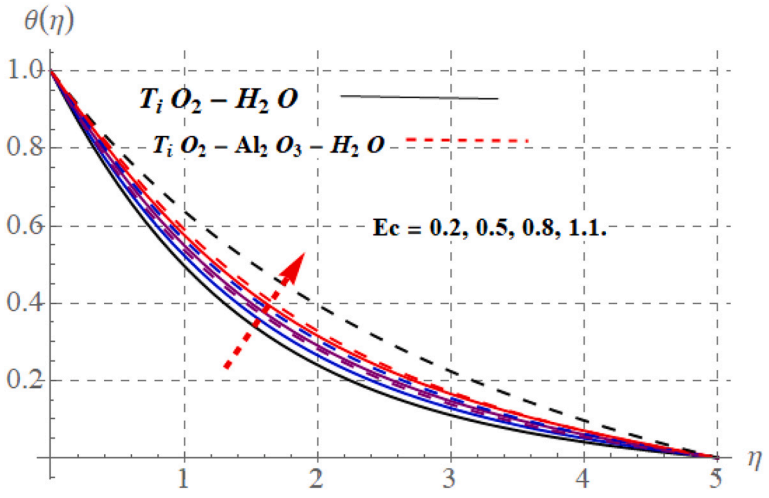

Fig. 7. $\theta(\eta)$ versus *Ec*.

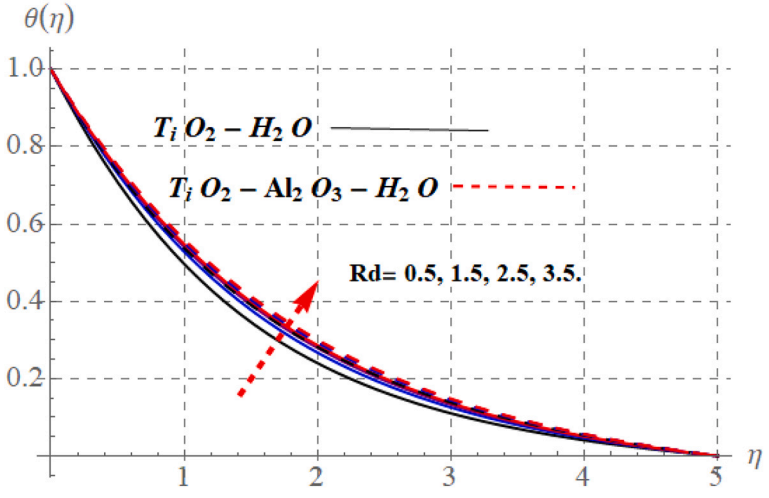

Fig. 8. $\theta(\eta)$ versus *Rd*.

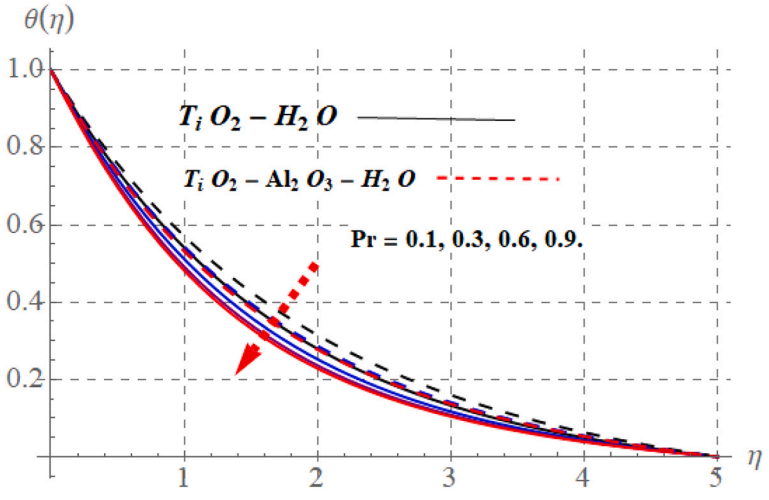

Fig. 9. $\theta(\eta)$ versus Pr.

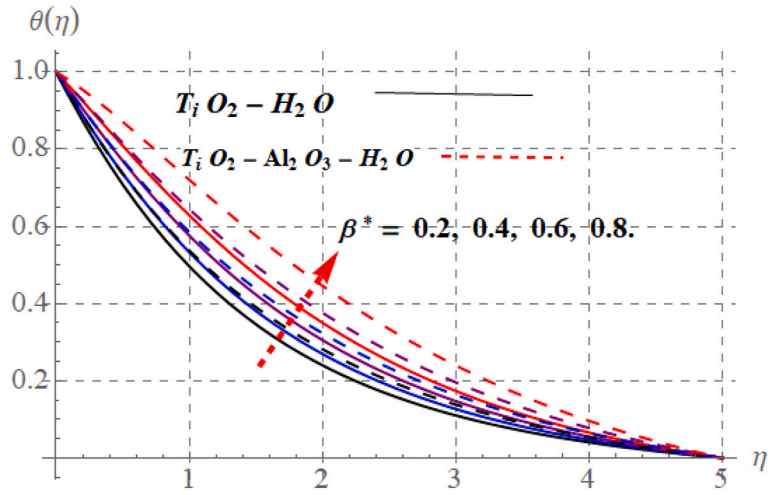

Fig. 10. $\theta(\eta)$ versus β^*.

Table 3
Computational outcomes of $Cf_x\sqrt{\mathrm{Re}_x}$ versus K^*, λ, H_{a^2} and K_1.

K^*	G_t	B	K_1	$-Cf_x\sqrt{\mathrm{Re}_x}(T_iO_2/H_2O)$	$-Cf_x\sqrt{\mathrm{Re}_x}(T_iO_2-Al_2O_3/H_2O)$
0.1	0.3	0.5	0.5	0.63299	0.985989
0.5				0.743644	1.11511
1.0				3.91637	1.2629
	0.5			0.534672	0.891344
	0.7			0.438139	0.798515
		1.0		0.184285	0.556915
		1.5		−0.233925	0.15874
			0.7	0.771765	1.12513
			0.9	0.899327	1.2547

Table 4
Computational outcomes of Nu_x versus K^*, λ, H_{a^2} and K_1.

K^*	Ec	Rd	Pr	β^*	$-Nu_x(T_iO_2/H_2O)$	$-Nu_x(T_iO_2-Al_2O_3/H_2O)$
0.1	0.2	0.5	0.5	0.1	0.385527	0.130382
0.5					0.551813	0.630628
1.0					0.79866	0.89382
	0.4				0.373656	0.393279
	0.6				0.361831	0.3691
		1.0			0.32161	0.360561
		1.5			0.28842	0.330213
			1.0		0.446587	0.469892
			1.5		0.476355	0.494537
				0.3	0.325342	0.318988
				0.5	0.256825	0.199918

3.2. Temperature

Figs. (6 − 9) are sketched to study the effect of K^*, Ec, Rd and Pr on temperature of single and hybrid nanofluid. Fig. 6 is outlined to explore the salient characteristics of $\theta(\eta)$ versus higher K^*. Temperature profile retards for rising K^*. Physically K^* has inverse relation with radius of cylinder, an increases in K^* reduces the radius of cylinder. As a result contact area between cylinder and fluid reduces. Thus temperature and thickness of thermal layer decays in both single and hybrid nanofluids via higher K^*. Impact of Ec on single and hybrid nanofluid is depicted in Fig.7. One can observe from Fig. 7, that higher Ec enhances temperature of single and hybrid nanofluid. Since kinetic energy and inter molecular movement in fluid increases for higher Ec. Due to which temperature field and associated layer thickness enhances in both cases. Fig. 8 is delineated to study the impact of radiation parameter on temperature of hybrid and single nanofluid. From Fig. 8 we conclude that temperature profile rises via higher Rd. Effect of Pr on $\theta(\eta)$ is sketched in Fig. 9. $\theta(\eta)$ diminishes for higher Pr values. It is due to the fact that Pr is ratio to momentum and thermal diffusivities. Thermal diffusivity decreases for higher Pr. Consequently, temperature and layer thickness decays for rising Pr values in both single and hybrid nanofluids. Fig. 10 shows the result of heat generation parameter on temperature field. It is depicted that temperature profile enhances for greater heat generation parameter.

3.3. Physical quantities

In this subsection computational values of skin friction $\left(Cf_x\sqrt{\mathrm{Re}_x}\right)$ and Nusselt number $\left(Nu_x\sqrt{\mathrm{Re}_x}\right)$ versus various parameters like K^*, G_t, K_1, B, Ec, Rd and Pr for both single and hybrid nanofluid are computed. Variation in $Cf_x\sqrt{\mathrm{Re}_x}$ for single and hybrid nanofluid versus higher K^*, G_t, B and K_1 are computed in Table 3. From table 3, we observe that magnitude of $Cf_x\sqrt{\mathrm{Re}_x}$ enhances versus K^* and K_1 whereas decays via higher G_t and B. Table 4 portrays the influence of K^*, Ec, Rd, Pr, and β^* on $Nu_x\sqrt{\mathrm{Re}_x}$ for single and hybrid nanofluid. It is noticed from Table 4 that Nusselt number diminishes via rising Ec, Rd and β^* while upsurges for higher K^* and Pr in both single and hybrid nanofluid.

4. Closing remarks

The main outcomes of current investigation are summarized as under:

- Decreasing effect of K^* on $f'(n)$ and $\theta(n)$ is observed.
- Opposite impact of K_1 and Gt on $f'(n)$ is noticed.
- $\theta(n)$ enhances via Ec, β^* and Rd while diminishes in case of Pr.
- Magnitude of $Cf_x\sqrt{\mathrm{Re}_x}$ enhances versus K^* and K_1 whereas decays via higher G_t and B.
- Nusselt number diminishes via rising Ec, Rd and β^* while upsurges for higher K^* and Pr.

Declaration of Competing Interest

The authors declare that they have no known competing financial interests or personal relationships that could have appeared to influence the work reported in this paper.

Acknowledgments

The research was supported by the National Natural Science

Foundation of China (Grant Nos. 11971142, 11871202, 61673169, 11701176, 11626101, 11601485).

References

[1] S.P.A. Devi, S.S.U. Devi, Numerical investigation of Hydromagnetic hybrid cu – Al2O3/water Nanofluid flow over a permeable stretching sheet with suction, International Journal of Nonlinear Sciences and Numerical Simulation 17 (5) (2016) 249–257.

[2] I. Waini, A. Ishak, I. Pop, Transpiration effects on hybrid nanofluid flow and heat transfer over a stretching/shrinking sheet with uniform shear flow, Alexandria Engineering Journal 59 (1) (2020) 91–99.

[3] M. Khan, S. Khan, T. Hayat, M. Waqas, A. Alsaedi, Modeling and numerical simulation for flow of hybrid nanofluid (SiO 2 /C 3 H 8 O 2) and (MoS 2 /C 3 H 8 O 2) with entropy optimization and variable viscosity, International Journal of Numerical Methods for Heat & Fluid Flow (2019), https://doi.org/10.1108/HFF-10-2019-0756 ahead-of-print.

[4] S.S. Ghadikolaei, K. Hosseinzadeh, M. Hatami, D.D. Ganji, MHD boundary layer analysis for micropolar dusty fluid containing hybrid nanoparticles (cu-Al2O3) over a porous medium, J. Mol. Liq. 268 (2018) 813–823.

[5] M.M. Maskeen, A. Zeeshan, O.U. Mehmood, M. Hassan, Heat transfer enhancement in hydromagnetic alumina–copper/water hybrid nanofluid flow over a stretching cylinder, J. Therm. Anal. Calorim. 138 (2) (2019) 1127–1136.

[6] M.I. Khan, M. Waqas, T. Hayat, A. Alsaedi, A comparative study of Casson fluid with homogeneous-heterogeneous reactions, J. Colloid Interface Sci. 498 (2017) 85–90.

[7] S.A. Khan, M.I. Khan, T. Hayat, A. Alsaedi, Darcy-Forchheimer hybrid (MoS2, SiO2) nanofluid flow with entropy generation, Comput. Methods Prog. Biomed. 185 (2020) 105152.

[8] R. Muhammad, M.I. Khan, N.B. Khan, M. Jameel, Magnetohydrodynamics (MHD) radiated nanomaterial viscous material flow by a curved surface with second order slip and entropy generation, Comput. Methods Prog. Biomed. 189 (2020) 105294.

[9] M. Rashid, T. Hayat, A. Alsaedi, Entropy generation in Darcy–Forchheimer flow of nanofluid with five nanoarticles due to stretching cylinder, Applied Nanoscience (2019) 9.

[10] S. Dinarvand, M. Rostami, I. Pop, A novel hybridity model for TiO2-CuO/water hybrid nanofluid flow over a static/moving wedge or corner, Sci. Rep. 9 (2019) 16290.

[11] S.S. Ghadikolaei, M. Gholinia, 3D mixed convection MHD flow of GO-MoS2 hybrid nanoparticles in H2O–(CH2OH)2 hybrid base fluid under the effect of H2 bond, International Communications in Heat and Mass Transfer 110 (2020) 104371.

[12] M.I. Khan, A. Alsaedi, T. Hayat, N.B. Khan, Modeling and computational analysis of hybrid class nanomaterials subject to entropy generation, Comput. Methods Prog. Biomed. 179 (2019) 104973.

[13] F. Kamal, K. Zaimi, A. Ishak, I. Pop, Stability analysis on the stagnation-point flow and heat transfer over a permeable stretching/shrinking sheet with heat source effect, International Journal of Numerical Methods for Heat & Fluid Flow. 28 (2018).

[14] D. Nor Fadhilah, N. Bachok, N. Yacob, N. Arifin, H. Rosali, Unsteady stagnation-point flow and heat transfer over a permeable exponential stretching/shrinking sheet in Nanofluid with slip velocity effect: a stability analysis, Appl. Sci. 8 (2018) 2172.

[15] T. Hayat, M. Ijaz, S. Qayyum, M. Ayub, A. Alsaedi, Mixed convective stagnation point flow of nanofluid with Darcy-Fochheimer relation and partial slip, Results in Physics 9 (2018) 771–778.

[16] M. Yousefi, S. Dinarvand, M. Yazdi, I. Pop, Stagnation-point flow of an aqueous titania-copper hybrid nanofluid toward a wavy cylinder, International journal of numerical methods for Heat & Fluid Flow (2018) 28.

[17] I. Waini, A. Ishak, I. Pop, Hybrid nanofluid flow towards a stagnation point on a stretching/shrinking cylinder, Sci. Rep. 10 (1) (2020) 9296.

[18] J. Ahmed, A. Shahzad, A. Farooq, M. Kamran, S.U.-D. Khan, S.U.-D. Khan, Radiative Heat Transfer in Homann Stagnation-Point Flow of Hybrid Nanofluid, 2020 (Applied Nanoscience).

[19] I. Kececioglu, Y. Jiang, Flow through porous Media of Packed Spheres Saturated with Water, J. Fluids Eng. 116 (1) (1994) 164–170.

[20] M. Hassan, M. Marin, A. Alsharif, R. Ellahi, Convective heat transfer flow of nanofluid in a porous medium over wavy surface, Phys. Lett. A 382 (38) (2018) 2749–2753.

[21] S.A.M. Mehryan, M.A. Sheremet, M. Soltani, M. Izadi, Natural convection of magnetic hybrid nanofluid inside a double-porous medium using two-equation energy model, J. Mol. Liq. 277 (2019) 959–970.

[22] A. Jarray, Z. Mehrez, A. El Cafsi, Mixed convection ag-MgO/water hybrid nanofluid flow in a porous horizontal channel, The European Physical Journal Special Topics 228 (12) (2019) 2677–2693.

[23] N.A.L. Aladdin, N. Bachok, I. Pop, Cu-Al2O3/water hybrid nanofluid flow over a permeable moving surface in presence of hydromagnetic and suction effects, Alexandria Engineering Journal 59 (2) (2020) 657–666.

[24] Yashkun, U., Zaimi, K., Abu Bakar Nor, a., Ishak, a., & Pop, I. MHD hybrid nanofluid flow over a permeable stretching/shrinking sheet with thermal radiation effect. International journal of numerical methods for Heat & Fluid Flow, Vol. ahead-of-print, No. ahead-of-print.

[25] S. Ahmad, M. Ijaz Khan, T. Hayat, M. Imran Khan, A. Alsaedi, Entropy generation optimization and unsteady squeezing flow of viscous fluid with five different shapes of nanoparticles, Colloids Surf. A Physicochem. Eng. Asp. 554 (2018) 197–210.

[26] M. Turkyilmazoglu, I. Pop, Heat and mass transfer of unsteady natural convection flow of some nanofluids past a vertical infinite flat plate with radiation effect, Int. J. Heat Mass Transf. 59 (2013) 167–171.